Title:

Transcriptomic analysis of brain hypometabolism links the cholinergic and gingipain hypotheses of Alzheimer's disease pathogenesis

Abstract

Alzheimer's disease (AD) starts decades before clinical symptoms appear. Low glucose utilization in regions of the cerebral cortex mark early AD and is informative for clinical diagnosis. To identify these specific regions, we conducted a meta-analysis of positron emission tomography studies that compared AD patients with healthy controls. Using the Allen Human Brain Atlas, we then identified genes with expression patterns associated with this hypometabolism map. Of the six brains in the Atlas, one demonstrated a strong spatial association with the hypometabolism pattern. Within this brain, genes encoding cytosolic ribosome proteins are highly expressed in the hypometabolic regions. Analyses of human and mouse data show that expression of these genes increases across AD-associated states of microglial activation, is high in acetylcholine-rich brain regions and neurons, and is up-regulated in inflamed gingival tissue. Taken together, our molecular characterization of cortical hypometabolism links the cholinergic and gingipain hypotheses of AD.

Author list:

Sejal Patel[1], Derek Howard[1], Alana Man[1,2], Deborah Schwartz[3,4], Joelle Jee[1,5], Daniel Felsky[1], Zdenka Pausova[6], Tomas Paus[4,7,8,9], Leon French[1,8,9,10]

1. Krembil Centre for Neuroinformatics, Centre for Addiction and Mental Health, Toronto, ON, Canada
2. Victoria College, University of Toronto, Toronto, Canada
3. Rotman Research Institute, Baycrest Centre for Geriatric Care, University of Toronto, Toronto, Ontario, Canada
4. Department of Psychology, University of Toronto, Toronto, Ontario, Canada
5. Faculty of Arts and Science, University of Toronto, Toronto, Canada
6. The Hospital for Sick Children, University of Toronto, Toronto, Ontario, Canada
7. Bloorview Research Institute, Holland Bloorview Kids Rehabilitation Hospital, Toronto, Ontario, Canada
8. Department of Psychiatry, University of Toronto, Toronto
9. Institute for Medical Science, University of Toronto, Toronto, Canada
10. Campbell Family Mental Health Research Institute, Centre for Addiction and Mental Health, Toronto, Canada

Introduction

Alzheimer's disease, one of the most prevalent neurodegenerative diseases, is thought to affect approximately 5% of those aged 60 years and above worldwide [1]. It is the most common form of dementia, which is clinically characterized by a severe decline in cognitive functioning and defined neuropathologically by the emergence and topographical progression of amyloid plaques, neurofibrillary tangles, and neuronal loss[2].

Currently, fluorodeoxyglucose positron emission tomography (FDG-PET) is a primary frontline tool for the diagnosis of dementia and its subtypes. FDG-PET uses a radioactive tracer - [^{18}F] fluorodeoxyglucose - to measure glucose metabolism within the brain [3], with altered cerebral glucose metabolism indicating AD with high sensitivity and specificity [4]. Importantly, patterns of hypometabolism can be seen in at-risk individuals decades before the development of symptoms [5–9]. This timing supports the concept that AD exists on a spectrum or continuum of pathologies that includes stages of subtle cognitive decline, mild cognitive impairment, and dementia [10,11]. Despite the clear link between metabolic changes measured by FDG-PET and risk for AD, it remains unclear which etiopathological mechanisms are responsible for driving these changes.

Using molecular data from the Allen Human Brain Atlas, we sought to characterize the pattern of regional hypometabolism found in the cerebral cortex of patients with AD. By integrating this atlas with a meta-analytic map of FDG-PET signal from over 1,500 AD patients and cognitively normal controls, we identified genes with spatial patterns similar to that of the lower glucose metabolism in the human brain. We performed our analysis genome-wide without a focus on candidate genes or specific molecular mechanisms to uncover any links with existing hypotheses about AD etiology. We also estimated cell-type proportions in the regions of hypometabolism to test for differences in specific cellular contributions. Genes associated with hypometabolism in the cerebral cortex were also characterized for specific expression across the entire brain and nervous system.

Methods

Meta analysis of Alzheimer's FDG-PET studies

We performed a meta-analysis of FDG-PET studies that compared, at rest, Alzheimer's patients with healthy controls. To compile a list of studies, a literature search was

conducted on studies from January 1985 to January 2012. We used the following search query: [FDG-PET OR positron emission tomography OR fluorodeoxyglucose OR glucose metabolism] AND [dementia]. Studies were examined to fulfill the following criteria: (1) original research papers available in English (no case studies or reviews); (2) participants examined using [18F] FDG-PET at rest (no functional tasks); (3) AD patients compared with age-matched healthy controls; (4) clinical diagnosis of AD using NINCDS-ADRDA [12] or DSM-III [13] criteria; and (5) whole-brain analyses (no region-of-interest analyses) conducted in standardized stereotaxic space with available coordinates. Each article was read twice to determine if the study met the inclusion criteria.

Coordinates of regional hypometabolism peaks from retained articles were used to create Activation Likelihood Estimation (ALE) maps using BrainMap's GingerALE application (www.brainmap.org/ale) [14]. This software assigns each voxel an activation likelihood estimate that is equal to the probability of at least one of the reported peaks of hypometabolism being located in that voxel [15]. To find distinct anatomical clusters, these voxelwise maps were clustered (min cluster extent = 500mm3; false discovery rate q= 0.05). The identified clusters were then used to determine an ALE threshold that marks which voxels are inside regions of hypometabolism.

Gene expression data

The Allen Human Brain Atlas provides a comprehensive transcriptional landscape of the adult human brain [16]. The Atlas was obtained from six individuals (five males, one female), with age ranging from 24 to 57 years. Custom 64K Agilent microarrays were used to assay genome-wide expression in 3,702 spatially-resolved samples (232 named brain regions). We also used the RNA-sequencing datasets that were generated on the Illumina HiSeq2000 platform. These RNA-sequencing data were quantified with transcripts per million (TPM) and assayed a subset of anatomic structures from two of the six brains. The Allen Institute normalized the data and adjusted for array-specific biases, batch, and dissection method. Microarray probes were filtered using quality control data provided by Miller et al. [17]. After this filtering, 31,452 probes remained of the 58,692 on the microarray.

Differential expression analyses

The microarray dataset was first used at the sample and donor level to identify genes that are differentially expressed in the regions of hypometabolism identified by the ALE-based analysis. Expression values were mean-averaged for genes with multiple probes, resulting in 15,143 genes. This analysis was restricted to samples from the cerebral cortex, as marked by the Allen Human Brain Atlas annotations (allocortical

regions, namely the hippocampal formation and piriform cortex, were excluded). For each donor and gene, expression values were compared between samples inside and outside of the hypometabolic regions using the Mann-Whitney U test. The Allen Institute provided MNI coordinates, which were used to map expression values into the voxel space of the meta-analysis. For analyses that spanned multiple donors, Fisher's method was used to generate a single meta p-value for each gene and direction [18]. We used the Benjamini–Hochberg false discovery rate (FDR) procedure for multiple test correction to adjust for the many tested genes [19].

Gene Ontology enrichment analysis

The Gene Ontology (GO) provides gene-level annotations that span specific cellular components, biological processes, and molecular functions [20]. These annotations, defined by GO terms, were required to have annotations for 10 to 200 tested genes (6,333 GO groups annotating 14,241 unique genes). To test for enrichment, we sorted the genes from the most overexpressed to underexpressed in regions of hypometabolism. Within this ranking, the area under the receiver operating characteristic curve (AUC) was used to test for gene ontology terms that are enriched in either direction (overexpressed: AUC > 0.5, underexpressed: AUC < 0.5). The Mann–Whitney U test was used to determine statistical significance with FDR correction for the GO groups tested. We used GO annotations from the GO.db and org.Hs.eg.db packages in R, version 3.8.2, which were dated April 24, 2019 [21,22]. We used the REVIGO tool to summarize many terms that were significant after correction [23]. We used the default REVIGO parameters with uncorrected p-values for the input GO groups and restricted this analysis to the biological process branch of the GO.

Estimation of Cell-Type Proportions

The Marker Gene Profile (MGP) tool was used to estimate cell-type proportions from the cerebral cortex expression profiles [24]. This method uses the first principal component of the expression of cell-type specific genes to estimate the relative abundance of a cell-type. We used 21 top marker genes obtained from a single cell study of the adult human temporal cortex [Supplementary Table S3 in [25]]. This study used transcriptomic profiles to cluster cells into astrocyte, neuron, oligodendrocyte, oligodendrocyte precursor, microglia and endothelial groups. These marker genes were used to calculate AUC values and estimate cell-type proportions with the MGP tool. Proportions were estimated separately for each donor across the same cortical samples used in the differential expression analysis.

Gene expression processing for anatomical enrichment analysis

In addition, the Allen Human Brain Atlas was used to determine regional enrichment of the genes identified in the differential expression analyses throughout the brain. Thus, in

contrast to the differential analyses that focused on samples from the cerebral cortex, this approach used the whole brain, and expression profiles were summarized to named brain regions. For each donor, samples mapping to the same-named brain region were mean-averaged to create a single expression profile for each region. Values from analogous named brain regions of both hemispheres were pooled because no significant differences in molecular architecture have been detected between the left and right hemispheres [17]. Expression levels of the 31,452 probes were then summarized by mean averaging for each of 15,126 gene transcripts. Expression values were next converted to ranks within a named brain region, and then z-score normalized across brain regions. For the analyses that combine across donors, z-scores for each donor were averaged to obtain a single gene-by-region reference matrix of expression values.

Mouse nervous system gene expression data

The RNA sequencing data that were used to characterize gene expression across the mouse nervous system were obtained from Zeisel et al. [26]. This dataset of more than 500,000 isolated cells from 19 defined regions was obtained from male and female mice that ranged in age from 12 to 56 days old. Following quality control, Zeisel et al. identified 265 clusters of cells. These clusters are thought to represent different cell types. Aggregate expression values for the identified transcriptomic cell-type clusters were obtained from the Mousebrain.org downloads portal. These values were log(expression+1) transformed and then z-scored at the gene level. We restricted our analysis to genes with human homologs by filtering mouse gene symbols for those that have human homologs [27]. Z-scores for expression are then ranked genome-wide within a defined cell-type cluster.

Neuroanatomical and cell-type cluster enrichment analysis

To calculate enrichment for gene sets of interest within a brain region or a cell type, z-scores in the processed expression matrices are first ranked. This provides a genome-wide list for each cell type or brain region with high ranks marking specific and low for depleted expression. We project our genes of interest into these ranked lists to determine enrichment. The AUC statistic was used to quantify if the genes of interest are more specifically expressed (ranked higher) in this sorted list of genes for a specific region or cell cluster. In this context, AUROC > 0.5 means the associated genes have specific or enriched expression in a brain region/cell-type cluster. For AUROC < 0.5 the reverse is true, with a bias toward lower relative expression. The Mann-Whitney U test was used to test the statistical significance and the FDR procedure was used to correct for testing of multiple brain regions or cell clusters within a dataset.

Single-cell RNA sequencing analysis of mouse microglia

Supplemental data from a single-cell RNA sequencing study of wild type and AD transgenic mouse model (5XFAD) were used to examine expression in immune cell types [28]. Keren-Shaul and co-authors profiled trancriptomically 8,016 immune cells from three wild type and three 5XFAD mice and clustered these cells into 10 distinct subpopulations based on expression. Of these 10 clusters, 3 expressed microglia markers. Two of these microglia clusters contained primarily cells from 5XFAD and not wild type mice and named them disease-associated microglia (DAM). For our analysis we consider these clusters separately as different microglial states: normal, intermediate (group II DAM), and AD associated (group III DAM).

Single-nucleus RNA sequencing analysis

Supplemental data from a single-nucleus RNA sequencing study of the human prefrontal cortex were used to examine differential expression across AD states in microglia. Specifically, for each gene we extracted adjusted p-values (IndModel.adj.pvals), mean expression, and fold changes (IndModel.FC) from Supplement Table 2 in Mathys, Davila-Velderrain, et al. [29]. After quality control, Mathys, Davila-Velderrain, et al. clustered the transcriptomes of 70,634 nuclei from 48 individuals into eight broad cell-type clusters. For this work we focused on data from the 1,920 microglia nuclei. The 48 participants in this study were classified into no (24), early (15) and late (9) AD pathology. To test for enrichment of our genes of interest, we sorted the genes from the most overexpressed to underexpressed for the differential expression results for no versus early pathology and early versus late pathology analyses. Within this ranking, the area under the receiver operating characteristic curve measure (AUC) was used to test for genes that are significantly enriched in either direction. We also used the mean expression to determine which genes increase in expression across the three pathology groups. For a given set of genes, the hypergeometric test was used to determine if a greater number of genes increase across pathology than expected by chance.

Results

Meta-analysis of FDG-PET studies of AD

Our literature search for FDG-PET studies identified 3,229 titles. Screening of the abstracts yielded 230 relevant studies. Upon review of the full articles, 29 relevant studies remained. When two studies utilized the same patient population, one of the overlapping studies was excluded, resulting in a total of 27 studies yielding 33

independent samples with a total of 915 Alzheimer's patients and 715 healthy controls (Supplement Table 1). ALE meta-analysis of these studies identified the following cortical regions as showing (consistently) lower glucose metabolism in patients vs. controls: posterior cingulate gyrus, middle frontal region, angular gyrus, middle and inferior temporal regions. A cluster analysis revealed 23 clusters (min cluster extent = 500mm3; FDR q= 0.05). A voxel-wise threshold of 0.006 was set to mirror this clustering map (Figure 1) and was used to determine if a given voxel was inside an AD-associated region of hypometabolism in subsequent transcriptomic analyses.

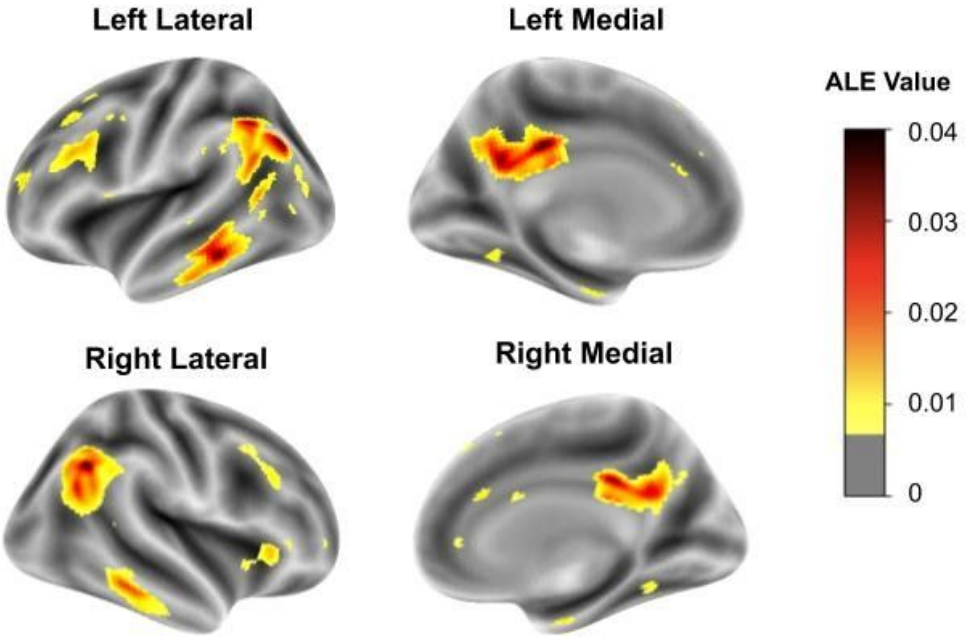

Figure 1: Cortical surface views of the ALE meta-analysis results. Regions where hypometabolism was not detected are transparent (ALE value of 0.006 or less). Lower glucose utilization (AD vs. controls) ranges from low (yellow) to high (black).

Many genes are differentially expressed in cortical regions with AD associated hypometabolism

Using all six brains included in the Allen Atlas, we first identified the genes that were differentially expressed in the FDG-PET-defined hypometabolic regions of the cerebral cortex (1 female and 5 male, aged 24–57 years). The number of cerebral cortex samples that were transcriptomic profiled by the Allen Institute ranged from 182 to 481 per donor; of those, 5.9-9.9% overlapped with the hypometabolic regions. Of the 15,143 genes tested, 99 were significantly expressed at higher, and 51 at lower levels in these

hypometabolic regions, after correction, across all donors. Substantial variability across the six brains in the Allen Human Brain Atlas has been previously noted both genome-wide and in the context of AD [30–33]. Given this variability, we then tested each brain separately. Strikingly, one brain drove the majority of the above atlas-wide signal for spatial expression overlap with the FDG-PET-derived map. In this brain (10021/H0351.2002), 647 genes were differentially expressed with 74% being expressed at lower levels in the hypometabolic regions (Supplement Table 2). In the remaining five donor brains, differentially expressed genes were only found in the oldest donor (donor 12876/H0351.1009, 57-year-old male). Taken together, our analysis of brain 10021/H0351.2002 marks it as an outlier with hundreds of genes that align spatially with the patterns of lower glucose metabolism observed in patients with AD (vs. controls).

Brain specific analyses point to a unique donor

We examined the demographic information and metadata of this donor to help understand the above observation. Brain 10021/H0351.2002 was from a 39-year-old male individual. Postmortem interval was 10 hours, the lowest of the six donors. In agreement, RNA Integrity values (RIN) for this brain are higher than the other donors for all four of the regions assayed for RIN (frontal pole: 7.5, occipital pole: 7.1, cerebellum: 8.6, and brainstem: 7.3). As documented by the Allen Institute, this donor, like the others, had no known history of neuropsychiatric or neurological conditions. The included brains were also classified as “normal” by a radiologist or pathologist. While considered “normal”, it was noted that brain 10021/H0351.2002 contained a single neurofibrillary tangle in the entorhinal cortex. Neurofibrillary tangles in the hippocampus and entorhinal cortex are considered early events in AD progression [34]. Neurofibrillary tangles were not found in the other five brains (three of which are older than this donor). The presence of a neurofibrillary tangle is a unique feature of this individual and the postmortem interval and RIN values suggest tissue quality is not driving the Alzheimer’s associated molecular patterns that are observed.

To distil the molecular results we performed GO enrichment analysis on the transcriptome-wide results from donor brain 10021/H0351.2002. In total, 215 GO groups were significantly enriched (Table 1 shows the top 10 GO terms enriched for genes upregulated in hypometabolic regions). Due to the high degree of overlap in gene membership among our top GO terms, we used REVIGO tool to summarize them [23]. This tool removes redundant GO terms based on semantic similarity, providing a dispensability metric. Of the 98 biological process terms enriched for overexpression, three were assigned the lowest possible dispensability score of zero: SRP-dependent cotranslational protein targeting to membrane (GO:0006614, 87 genes, AUC = 0.874,

$p_{FDR} < 10^{-28}$), chronic inflammatory response (GO:0002544, 15 genes, AUC = 0.78, $p_{FDR} < 0.05$), and cell killing (GO:0001906, 94 genes, AUC = 0.60, $p_{FDR} < 0.05$). The strongest signal is from genes involved in SRP-dependent cotranslational protein targeting to membrane (Figure 2). This process targets protein translocation to the endoplasmic reticulum via the signal-recognition particle (SRP). These genes are primarily components of the cytosolic ribosome and henceforth referred to as 'ER translocation' genes. Six of these genes are found within the top 20 genes with higher expression in hypometabolic regions (*RPL34*, *RPL32*, *RPS27*, *RPS27A*, *RPL37A*, and *RPS15A*). In contrast, genes that are underexpressed in regions of hypometabolism are less significantly enriched for specific GO terms (lowest $p_{FDR} = 7.3 \times 10^{-8}$). However, these top terms contain more diverse themes (Table 2), some of which have been previously implicated in AD. The most significant GO terms representing these themes are: 'ubiquitin ligase complex', 'tRNA aminoacylation', 'ATPase activity, coupled', 'HOPS complex' (involved in endosomal vesicle tethering), and 'microtubule organizing center part'. The ubiquitin-proteasome system has been linked to AD [35]. Of the four genes that encode ubiquitin, three with available data are strongly overexpressed in regions of hypometabolism in this brain. In summary, this enrichment analysis points to spatial differences in vesicle fusion, protein translation, targeting, and degradation.

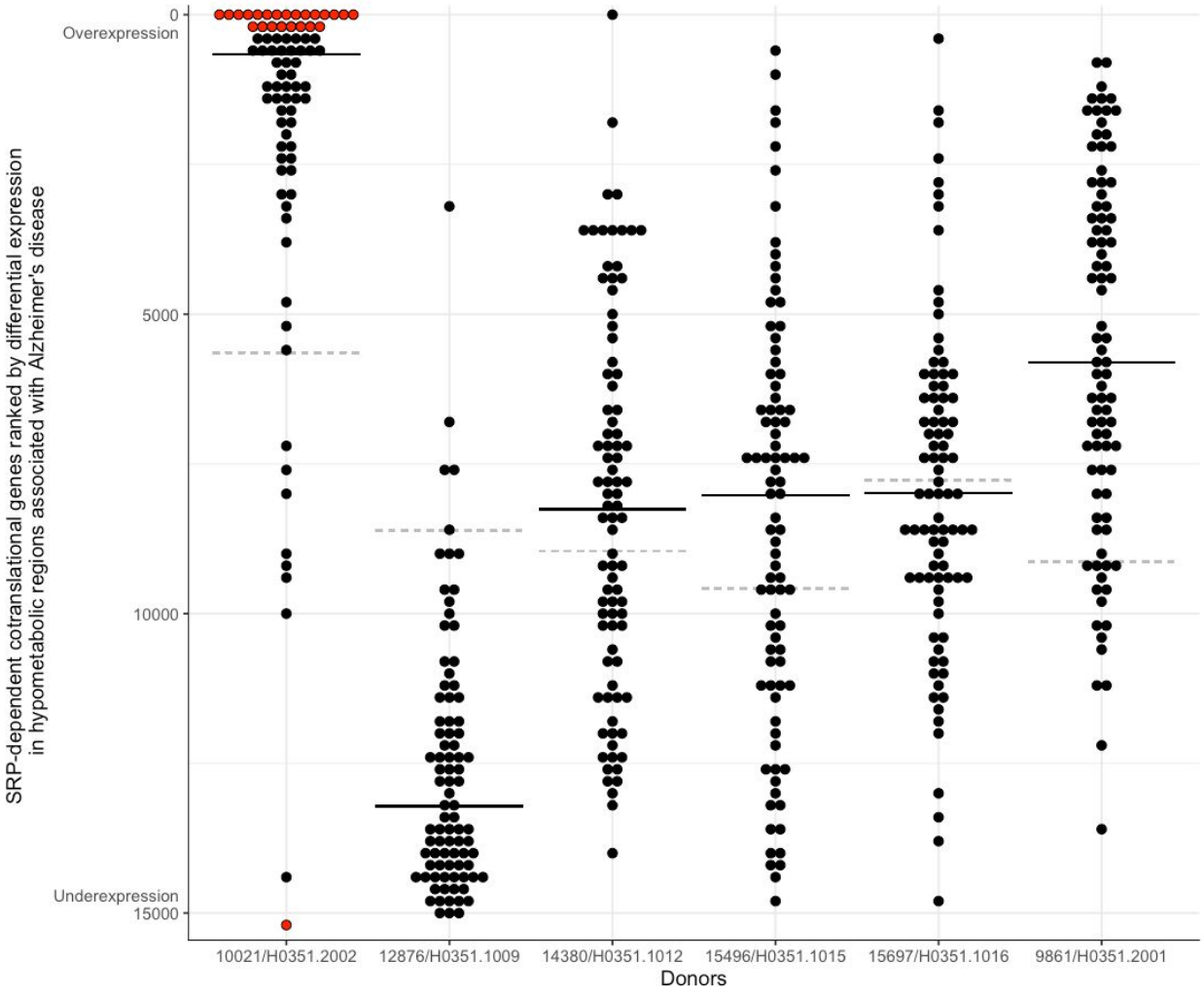

Figure 2: SRP-dependent cotranslational genes ranked based on differential expression in hypometabolic regions associated with AD. Genes are marked with dots, with the y-axis representing the genome-wide differential expression rank and ranges from overexpression (top) to underexpression (bottom). The black line marks the median expression rank of the SRP-dependent cotranslational genes. The dashed grey line marks the gene with the most stable expression between inside and outside of the hypometabolic regions for each donor. Red highlights genes that pass correction for multiple testing.

Table 1: Top ten GO groups enriched for overexpression in areas of Alzheimer's associated hypometabolism in brain 10021/H0351.2002.

Name	Genes	ID	AUC	$p\text{-value}_{FDR}$
SRP-dependent cotranslational protein targeting to	87	GO:0006614	0.874	1.35E-29

membrane				
cotranslational protein targeting to membrane	90	GO:0006613	0.865	2.07E-29
protein targeting to ER	92	GO:0045047	0.847	2.86E-27
cytosolic ribosome	87	GO:0022626	0.856	3.45E-27
establishment of protein localization to endoplasmic reticulum	96	GO:0072599	0.828	1.66E-25
structural constituent of ribosome	107	GO:0003735	0.794	1.05E-22
ribosomal subunit	158	GO:0044391	0.737	1.01E-21
nuclear-transcribed mRNA catabolic process, nonsense-mediated decay	104	GO:0000184	0.783	2.07E-20
protein localization to endoplasmic reticulum	109	GO:0070972	0.765	9.44E-19
cytosolic large ribosomal subunit	47	GO:0022625	0.894	6.73E-18

Table 2: Top ten GO groups enriched for underexpression in areas of Alzheimer's associated hypometabolism in brain 10021/H0351.2002.

Name	**Genes**	**ID**	**AUC**	**p-value$_{FDR}$**
ubiquitin ligase complex	195	GO:0000151	0.368	7.35E-08
tRNA aminoacylation	42	GO:0043039	0.259	1.91E-05
cullin-RING ubiquitin ligase complex	111	GO:0031461	0.355	3.84E-05
amino acid activation	43	GO:0043038	0.275	8.24E-05
aminoacyl-tRNA ligase activity	33	GO:0004812	0.243	8.24E-05
tRNA aminoacylation for protein translation	40	GO:0006418	0.268	9.84E-05
ATPase activity, coupled	186	GO:0042623	0.396	0.00026
HOPS complex	13	GO:0030897	0.137	0.00135
DNA-dependent ATPase activity	59	GO:0008094	0.33	0.00145
microtubule organizing center part	145	GO:0044450	0.395	0.00244

To test if regional transcriptomic differences might be due to cell type proportions, we performed enrichment analyses of cell type-specific marker genes based on the

differential expression results. In the five brains, microglia marker genes were expressed at low levels in the hypometabolic regions (underexpressed; AUC = 0.1, $p_{FDR} < 10^{-8}$) while astrocyte and neuron markers were expressed at high levels (overexpressed; AUC > 0.66, $p_{FDR} < 0.05$). In contrast, brain 10021/H0351.2002 showed an opposite pattern of enrichment (Supplement Table 3). Using the Marker Gene Profile [24] tool, which uses a more complex parametric method, we also observe an interaction between hypometabolic regions and brain 10021/H0351.2002, whereby estimates of microglia proportions are higher inside hypometabolic regions in brain 10021/H0351.2002 (5 genes, t = 2.1, p = 0.033) and estimated proportions of neurons are lower (21 genes, t = -4.0, p < 0.0001).

Focusing on donor 10021/H0351.2002, the top-ranked gene ontology group, 'SRP-dependent cotranslational protein targeting to membrane'/'ER translocation', contains genes that are involved in the targeting of proteins to the endoplasmic reticulum. Upon literature search, we found no strong evidence that this mechanism was associated with beta-amyloid or tau deposition. Motivated by findings linking AD to *P. gingivalis* infection [36,37], we searched for studies linking ER translocation genes and periodontitis (*P. gingivalis* is a key periodontal pathogen). We found a spatial transcriptomics study that reported higher expression of the ER translocation genes in inflamed areas of periodontitis-affected gingival connective tissue compared to non-inflamed areas [38]. A second study that examined peri-implant soft tissue also found that ER translocation genes are expressed at higher levels in diseased mucosa samples [39]. Given these links to *P. gingivalis* infection, we pursued further characterization of the ER translocation genes.

Given the high and ubiquitous expression of ribosomal genes, it is possible that the ER translocation signal is due to ceiling effects induced by the dynamic range of microarray gene expression profiling. To address this concern, we tested for the association using RNA sequencing data, which has a broader dynamic range. We again observe that the ER translocation genes are enriched (100 cerebral cortex samples, AUC = 0.733, $p_{FDR} < 10^{-9}$). While limited in sample coverage for donor 10021/H0351.2002, the RNA sequencing data validates the finding of differential expression of ER translocation genes.

ER translocation genes are highly expressed in the substantia innominata

We limited our preceding analysis to the cerebral cortex because of the limited resolution of FDG-PET images. Here we sought to characterize the brain-wide expression profile of the ER translocation genes, independent of the FDG-PET pattern. In this analysis, for a given brain region, the genome was ranked from the most

specifically expressed gene to the most depleted gene, relative to the rest of the brain. In a combined analysis of all six brains, 86 of the 232 brain regions showed an overexpression of the ER translocation genes. Of those, the substantia innominata was top ranked with the most specific expression of the ER translocation genes (AUC = 0.841, $p_{FDR} < 10^{-26}$, full listing in Supplement Table 4). Of the nine remaining top 10 regions, six are located near the substantia innominata: nucleus accumbens, the septal nuclei, substantia nigra pars reticulata, internal and external globus pallidus, and the paraterminal gyrus (AUCs > 0.761, all $p_{FDR} < 10^{-15}$). Given the differences between the donors, we performed this analysis for each donor individually. The substantia innominata is the 11th ranked brain region (of 194) for selective expression of ER translocation associated genes in donor 10021/H0351.2002, and is ranked 2nd of 182 in donor 9861/H0351.2002. There are no samples from the substantia innominata in the other four donors, but its constituent nuclei are. Testing for anatomical enrichment of the ER translocation associated genes in these nuclei reveals a highly heterogeneous pattern (Figure 3). A key characteristic of the substantia innominata is a high proportion of cholinergic neurons [40]. AD has been previously associated with cholinergic neuron loss in the basal forebrain and deficits in Choline O-Acetyltransferase (encoded by *CHAT*) [41–43]. Figure 3 shows the relationships between CHAT gene expression and ER translocation genes across the brain, marking the substantia innominata as having high expression of both *CHAT* and the ER translocation genes.

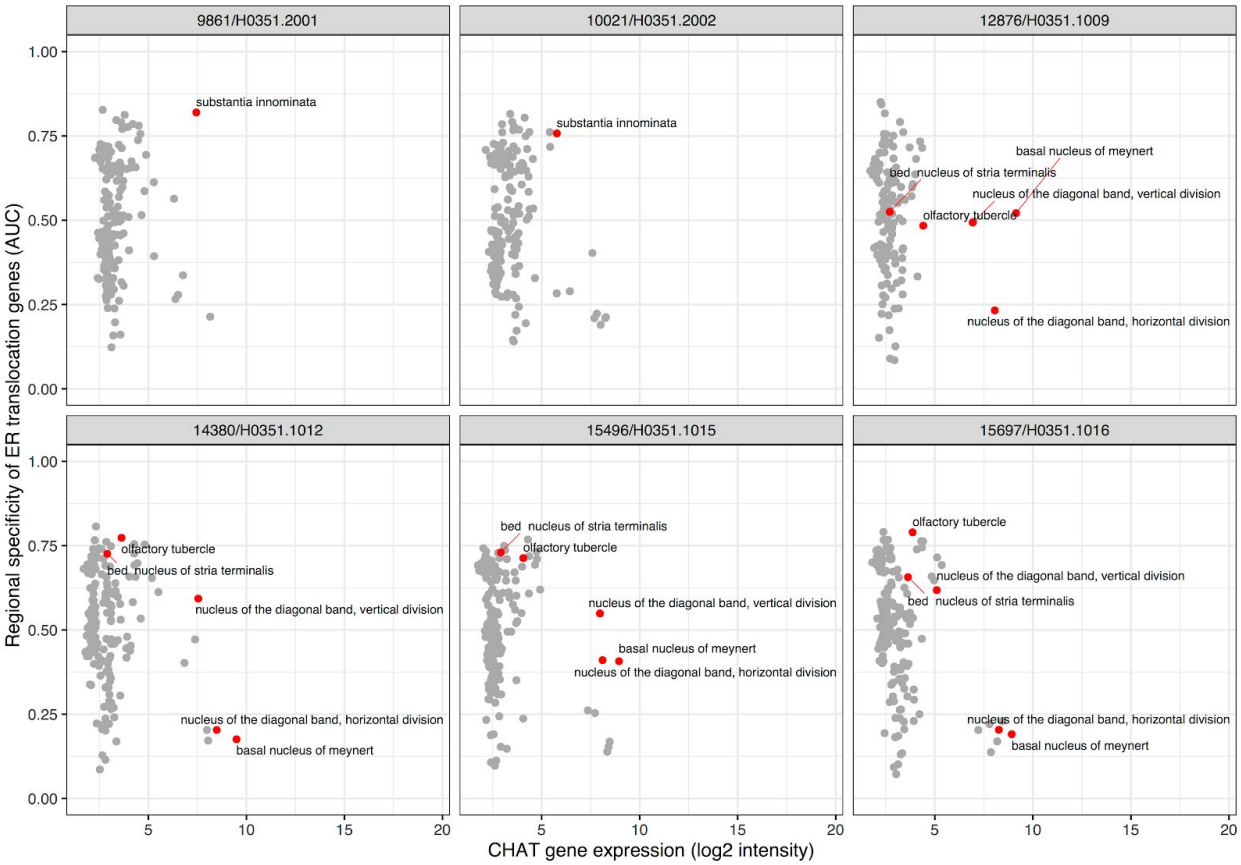

Figure 3: Scatter plots showing specific enrichment for ER translocation genes (y-axis) and Choline O-Acetyltransferase (*CHAT*) gene expression on the x-axis in each brain. Each point is a brain region with red marking the substantia innominata, and its nuclei.

ER translocation genes are highly expressed in mouse cholinergic neurons

We next characterized the expression patterns of the ER translocation genes at a finer resolution in the mouse nervous system [26]. Similar to the regional data from the Human Brain Atlas, we ranked each gene from the most specific to depleted expression across transcriptomic cell type clusters. We observe that the 74 mouse homologs of the ER translocation genes are not evenly expressed across clusters in this mouse single-cell atlas ($p_{FDR} < 0.05$, Supplement Table 5). Guided by the substantia innominata results, we filtered these results for cell clusters annotated as cholinergic. Four cholinergic enteric neuron clusters are within the top ten cell clusters. Of the 14 cholinergic clusters, 12 are enriched for ER translocation gene expression (AUC > 0.5, Table 3). Relative to the 265 cell type clusters, the cholinergic groups are enriched for higher AUC values ($p < 0.0001$, Mann-Whitney U test). The top-ranked cholinergic cell clusters from brain tissue are listed as telencephalon interneurons with an annotated location of striatum and amygdala (TECHO, AUC = 0.82, ranked 23). While substantia innominata is not

mentioned in this dataset, both the mouse and human regional analyses highlight the striatum and cholinergic system.

Table 3. ER translocation gene enrichment statistics for cholinergic transcriptomic cell type clusters.

Cluster_ID	Name	AUC	pValue	p_{FDR}	Rank
ENT5	Cholinergic enteric neurons	0.922	4.02e-36	1.18e-34	1
ENT6	Cholinergic enteric neurons	0.879	2.21e-29	1.89e-28	4
ENT8	Cholinergic enteric neurons, VGLUT2	0.873	1.33e-28	1.01e-27	5
ENT4	Cholinergic enteric neurons	0.862	5.95e-27	3.94e-26	9
TECHO	Cholinergic interneurons, telencephalon	0.817	4.34e-21	1.86e-20	23
ENT7	Cholinergic enteric neurons, VGLUT2	0.804	1.54e-19	5.91e-19	28
ENT9	Cholinergic enteric neurons	0.787	1.4e-17	4.47e-17	36
SYCHO2	Cholinergic neurons, sympathetic	0.773	5.47e-16	1.56e-15	40
SYCHO1	Cholinergic neurons, sympathetic	0.734	3.57e-12	7.76e-12	57
DECHO1	Cholinergic neurons, septal nucleus, Meynert and diagonal band	0.729	9.3e-12	1.94e-11	60
DECHO2	Cholinergic neurons, habenula	0.705	1.19e-09	2.2e-09	73
MBCHO1	Cholinergic neurons, midbrain red nucleus	0.652	6.59e-06	9.98e-06	88
HBCHO1	Cholinergic neurons, hindbrain	0.513	0.705	0.721	132
HBCHO2	Cholinergic neurons, hindbrain	0.496	0.897	0.904	138

ER translocation gene expression is high in AD-associated microglia (DAM)

Based on the high expression of these genes in inflamed periodontal tissue and differential expression of microglia markers in donor 10021/H0351.2002, we examined the ER translocation genes in microglia from an Alzheimer's mouse model. We tested if the ER translocation genes increase in a stepwise pattern across the normal, intermediate, and full DAM clusters. For the 12,712 genes with data available, 6.5% monotonically increase in expression across these cell type clusters that represent distinct states. Of the 80 mouse homologs of the ER translocation genes, 75% increase in a stepwise fashion (Figure 4, hypergeometric $p < 10^{-52}$). Compared with all gene ontology groups, this is the most significant enrichment (Supplement Table 6). In this

single-cell dataset, ER translocation genes are expressed in AD associated microglia in a progressive pattern.

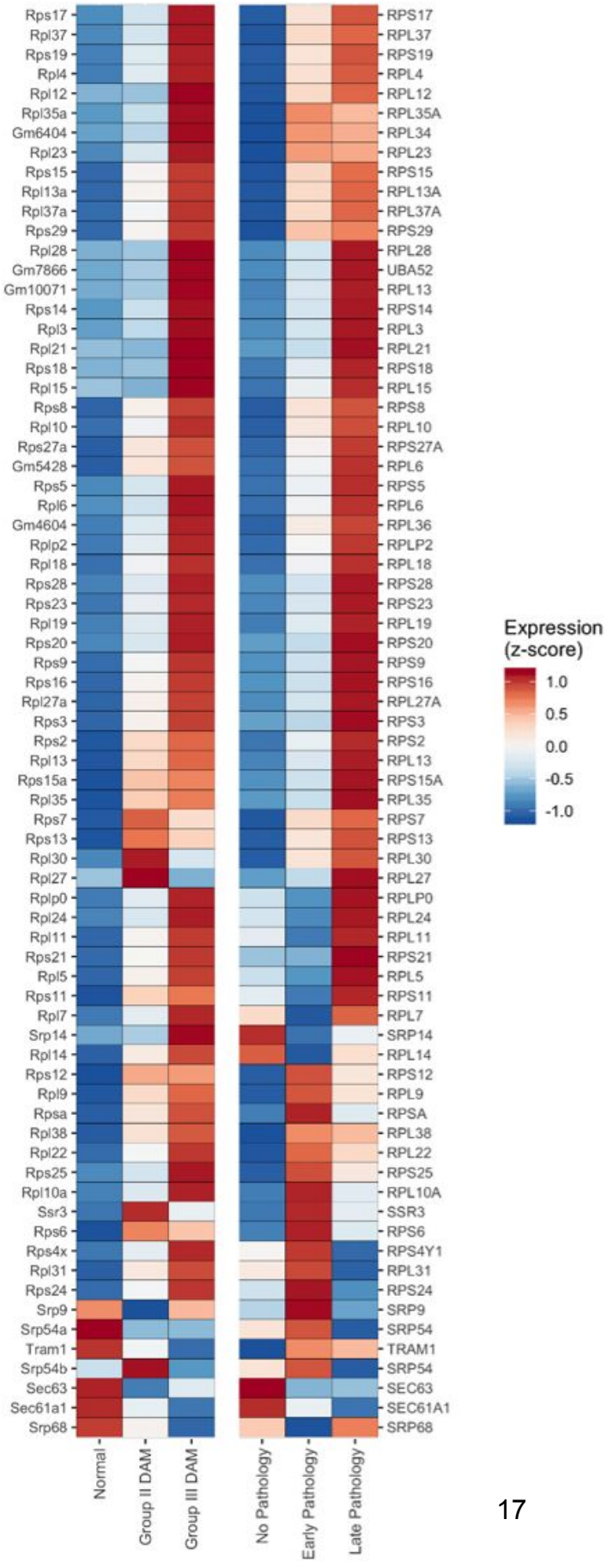

Figure 4. Heatmap of the ER translocation gene expression across three microglia cell clusters from AD mouse model (left half) and AD pathology subgroups (right half). Expression for each gene is z-scored with high expression in red and low in blue. Genes are ordered based on hierarchical clustering using complete linkage (genes with similar expression across the mouse and human data are clustered together). Three human genes are duplicated because they have two homologous mouse genes (*RPL6*, *RPL13*, and *SRP54*). Human genes without homologous mouse genes are not displayed.

Expression of ER translocation genes is correlated with AD pathology

Using data from a single-nucleus study of the human prefrontal cortex, we next tested if the ER translocation genes are differentially expressed across stages of AD pathology [29]. Guided by our findings in mouse, we restricted our analyses to microglia. When comparing expression between no- and early-pathology subgroups we find that the ER translocation genes are enriched for higher expression in microglia from the early pathology individuals (Supplement Figure 1, 79 genes, AUC = 0.716, $p < 10^{-10}$). For the comparison between early- and late-pathology subgroups, the ER translocation genes are also enriched for higher expression in the late-pathology microglia (Supplement Figure 1, 77 genes, AUC = 0.627, $p < 0.0005$). Beyond these pairwise tests, we counted how many genes increase with disease progression. Broadly, for the 7,319 genes with data available, average microglial expression of 17.9% progressively increase across the pathological groups. For the ER translocation genes, this proportion triples to 55.8% (Figure 4, 43 of 77 genes progressively increase, hypergeometric $p < 10^{-13}$). Compared to all GO groups, this is the second most significant group with the mostly overlapping set of cytosolic ribosome genes ranked first (Supplement Table 7). In this single-nucleus dataset, microglial expression of ER translocation genes is correlated with AD progression.

Discussion

In this study, we projected the transcriptome of the cerebral cortex onto the spatial pattern of glucose hypometabolism found in AD cases. Of the six normal brains we tested, only one demonstrated a strong spatial association between gene expression and the hypometabolism pattern. ER translocation genes, which encode proteins of the cytosolic ribosome and are involved in targeting protein translation to the endoplasmic reticulum, best align with the hypometabolic pattern in this brain. Using the transcriptomic data for this individual, we estimate a lower proportion of neurons and more microglia in hypometabolic regions. In support, prior neuropathological examination of this individual found a neurofibrillary tangle. The ER translocation genes

link both the cholinergic and gingipain hypotheses of AD. Specifically, these genes are highly expressed in diseased periodontal tissue [38,39], the substantia innominata, and cholinergic neurons. More directly, in microglia, the same genes have a staged expression pattern that increases across cellular and pathological AD associated states.

It is plausible that brain atlases seeking to assay the normal brain may contain samples from donors who may be in the hypothetical stage of preclinical AD [44]. This stage - when clinical symptoms are not yet present - may have started with periodontitis that may lead to *P. Gingivalis* breaching the blood-brain barrier [37]. Our findings suggest that donor 10021/H0351.2002 may have been on this path.

It is striking that the ER translocation GO group was the most significantly enriched set in our analysis of the 10021/H0351.2002 donor brain, AD associated microglia, and two previous studies of diseased periodontal tissue [38,39]. It is known that cytosolic ribosome genes are strongly co-expressed [45]. While we did not perform co-expression analysis, a change across this gene set will be easily detected with pathway or gene ontology analyses due to their high co-expression. This coherence is partly why it ranks above all other gene sets tested. Nonetheless, we note that a *RPL34* is a top ranked gene, providing a strong signal at the level of single genes. To gauge the chance of this GO group being top-ranked in multiple studies, we checked if the group is multifunctional or contains genes that are commonly differentially expressed. We found that this group ranked average in terms of multifunctional genes, relative to other groups (ranked 6,848th of 11,404 GO groups) [46]. In addition, this group was not top-ranked in any of the 635 studies systematically examined in a broad study of differential gene expression predictability [47]. More directly, the ER translocation genes are stable, with a below average prior probability of differential expression (ER translocation genes median = 0.246, remaining genes = 0.562, Mann-Whitney U test $p < 10^{-9}$). Therefore, while ER translocation genes are strongly co-expressed, the prior likelihood of the ER translocation genes being differentially expressed in the periodontal studies and our results is low.

ER translocation genes primarily encode proteins that make up the cytosolic ribosome. The ribosome and protein synthesis have been previously associated with mild cognitive impairment and AD [48–51]. Pathological tau has also been shown to determine translational selectivity and co-localize with ribosomes [52,53]. It has been postulated that tau fibrillization may block cytoskeleton-trafficking infections agents [54]. While speculative, the ER translocation genes point to mechanisms that link the gingipain hypothesis of AD. The gingipain hypothesis proposes that *Porphyromonas gingivalis* (*P. gingivalis*) infection of brain tissue causes AD [36,37]. In infected human cells, *P. Gingivalis*

is found in vacuoles that contain undegraded ribosomes [55]. Cytosolically free *P. gingivalis* quickly localizes to the rough endoplasmic reticulum to form these autophagosome-like vacuoles [56]. However, it is not known how *P. gingivalis* traffics to the endoplasmic reticulum [57]. SRP-dependent cotranslational protein targeting to the membrane may be exploited by *P. gingivalis* to reach the endoplasmic reticulum. Sequestration of ribosomes by *P. Gingivalis* may cause increased transcription of cytosolic ribosomal protein genes because ribosome biogenesis is highly regulated [58]. Further study is needed to experimentally test if *P. Gingivalis* exploits cytosolic ribosomes and ER translocation pathways.

Beyond the ER translocation genes, we note other GO groups with functional links to *P. gingivalis*. For example, ‘chronic inflammatory response’ and ‘cell killing’ genes were enriched for overexpression in the hypometabolic regions in brain 10021/H0351.2002. In the other direction, the genes in the homotypic fusion and protein sorting (HOPS) complex are underexpressed in hypometabolic regions in brain 10021/H0351.2002. This complex contains vacuole sorting genes and regulates autophagosome-lysosome fusion [59]. Experiments in endothelial cells have demonstrated that *P. gingivalis* is able to prevent the conversion of the autophagosome like vacuoles it is contained in [55]. Bypassing the maturation step from autophagosome to autolysosome allows its survival [57] and may involve downregulation of the HOPS complex. The top two most underexpressed gene sets in the hypometabolic regions are ‘ubiquitin ligase complex’ and ‘tRNA aminoacylation’. While ubiquitin ligase complex genes are underexpressed, genes encoding ubiquitin are overexpressed in the hypometabolic regions in brain 10021/H0351.2002. In postmortem samples of the temporal gyrus from neurologically normal individuals and Alzheimer’s patients, ubiquitin was correlated with levels of gingipains [36]. Like the cytosolic ribosome, these genes function in the protein life-cycle. *P. gingivalis* disrupts the protein life-cycle as it secretes proteases (gingipains) and ferments amino acids for energy [60]. These top-ranked gene sets connect the gingipain hypothesis of AD.

Extensive loss of cholinergic neurons in the substantia innominata has been found in Alzheimer's patients [61,62]. This finding and many others form the basis of the cholinergic hypothesis of AD which proposes that degeneration of cholinergic neurons in the basal forebrain substantially contributes to cognitive decline in AD patients [42]. This subcortical degeneration is thought to occur early in the disease process [63]. In the context of the gingipain hypothesis, we note that reduced basal forebrain volume and cholinergic function follow after the removal of teeth in rodents [64–66]. The ER translocation genes, which are strongly aligned with the hypometabolism pattern in brain 10021/H0351.2002 are highly expressed in the substantia innominata. In support of this link, basal forebrain

atrophy is positively correlated with cortical hypometabolism in individuals with mild cognitive impairment [67]. In a mouse single-cell atlas we found high expression of the ER translocation genes in cholinergic neurons, reinforcing the link to the cholinergic hypothesis. High expression of the ER translocation genes in cholinergic neurons may be required to support processing of acetylcholinesterase in the ER [68]. Cholinergic neurons in the enteric nervous system had the highest expression of the ER translocation genes. In the context of AD, loss of enteric cholinergic neurons has been observed in a transgenic mouse model of the disease [69]. Taken together, the ER translocation genes highlight cholinergic neurons and the substantia innominata, providing an anatomical link to the cholinergic hypothesis.

Beyond the Alzheimer's associated patterns in brain 10021/H0351.2002, we show that high ER translocation gene expression is observed in microglia from individuals with AD pathology. This is supported by a similar staged microglial expression pattern in a mouse model of AD. These findings do not link directly the cholinergic or gingipain hypotheses. However, we note that the gene most differentially expressed between normal and DAM microglia is cystatin F (*Cst7*). Similarly, cystatin C (*CST3*), is the fourth most differentially expressed gene in the comparison between early and late AD microglia profiles [29]. Previous studies have found that cystatin C is neuroprotective in AD [70]. Cystatins are cysteine protease inhibitors with the potential to block gingipains [71]. More directly, cystatin C is high in gingival crevicular fluid and serum of individuals with chronic periodontitis and is correlated with severity [72]. Cystatin C was also found to inhibit the growth of *P. gingivalis* and is functionally modified by gingipains [73,74]. In the DAM microglia study, the authors knocked out *Trem2* to reveal restricted neurodegeneration in their mouse model of AD. In humans, *TREM2* is genetically associated with AD [75]. While indirect, this gene suggests a link to infection through its function as a phagocytic receptor for bacteria [76]. While our microglia findings do not directly test the gingipain hypothesis, the cystatins and *TREM2* associations are supportive.

Acknowledgements

We thank Navona Calarco for help with the analysis of the single-cell atlas of the mouse nervous system, and Spiro Pantazatos for analyzing MRI scans. We thank the Allen Institute for Brain Science for creating the transcriptomic atlas of the human brain. We thank Ed Lein, Michael Hawrylycz, Jeremy Miller, and Shreejoy Tripathy for their insightful comments and suggestions.

This study was supported by the CAMH Foundation, CAMH Discovery Fund, and a National Science and Engineering Research Council of Canada (NSERC) Discovery Grant to LF.

Data availability

Scripts, supplementary tables, and data files for reproducing the analyses are available online at https://figshare.com/articles/Transcriptomic_analysis_of_brain_hypometabolism_links_the_cholinergic_and_gingipain_hypotheses_of_Alzheimer_s_disease_pathogenesis/9887438 and https://github.com/leonfrench/AD-Allen-FDG .

Conflict of Interest

LF owns shares in Cortexyme Inc., a company that is targeting *P. Gingivalis* with a gingipain inhibitor to treat AD. The other authors declare no conflict of interest.

References

1. Qiu, C., Kivipelto, M. & von Strauss, E. Epidemiology of Alzheimer's disease: occurrence, determinants, and strategies toward intervention. *Dialogues Clin. Neurosci.* **11**, 111–128 (2009).
2. Masters, C. L. *et al.* Alzheimer's disease. *Nature Reviews Disease Primers* vol. 1 (2015).
3. Friedland, R. P. *et al.* Regional cerebral metabolic alterations in dementia of the Alzheimer type: positron emission tomography with [18F]fluorodeoxyglucose. *J. Comput. Assist. Tomogr.* **7**, 590–598 (1983).
4. Mosconi, L. *et al.* Multicenter standardized 18F-FDG PET diagnosis of mild cognitive impairment, Alzheimer's disease, and other dementias. *J. Nucl. Med.* **49**, 390–398 (2008).
5. Mosconi, L. *et al.* Hypometabolism exceeds atrophy in presymptomatic early-onset familial Alzheimer's disease. *J. Nucl. Med.* **47**, 1778–1786 (2006).
6. Chen, K. *et al.* Correlations between FDG PET glucose uptake-MRI gray matter volume

scores and apolipoprotein E ε4 gene dose in cognitively normal adults: a cross-validation study using voxel-based multi-modal partial least squares. *Neuroimage* **60**, 2316–2322 (2012).

7. Reiman, E. M. *et al.* Functional brain abnormalities in young adults at genetic risk for late-onset Alzheimer's dementia. *Proc. Natl. Acad. Sci. U. S. A.* **101**, 284–289 (2004).
8. Landau, S. M. *et al.* Associations between cognitive, functional, and FDG-PET measures of decline in AD and MCI. *Neurobiol. Aging* **32**, 1207–1218 (2011).
9. Langbaum, J. B. S. *et al.* Hypometabolism in Alzheimer-Affected Brain Regions in Cognitively Healthy Latino Individuals Carrying the Apolipoprotein E ε4 Allele. *Arch. Neurol.* **67**, 462–468 (2010).
10. Albert, M. S. *et al.* The diagnosis of mild cognitive impairment due to Alzheimer's disease: recommendations from the National Institute on Aging-Alzheimer's Association workgroups on diagnostic guidelines for Alzheimer's disease. *Alzheimers. Dement.* **7**, 270–279 (2011).
11. McKhann, G. M. *et al.* The diagnosis of dementia due to Alzheimer's disease: recommendations from the National Institute on Aging-Alzheimer's Association workgroups on diagnostic guidelines for Alzheimer's disease. *Alzheimers. Dement.* **7**, 263–269 (2011).
12. McKhann, G. *et al.* Clinical diagnosis of Alzheimer's disease: report of the NINCDS-ADRDA Work Group under the auspices of Department of Health and Human Services Task Force on Alzheimer's Disease. *Neurology* **34**, 939–944 (1984).
13. American Psychiatric Association. *DSM-III-R*. (American Psychiatric Association, 1987).
14. Eickhoff, S. B. *et al.* Coordinate-based activation likelihood estimation meta-analysis of neuroimaging data: a random-effects approach based on empirical estimates of spatial uncertainty. *Hum. Brain Mapp.* **30**, 2907–2926 (2009).
15. Turkeltaub, P. E., Eden, G. F., Jones, K. M. & Zeffiro, T. A. Meta-analysis of the functional

neuroanatomy of single-word reading: method and validation. *Neuroimage* **16**, 765–780 (2002).

16. Hawrylycz, M. J. *et al.* An anatomically comprehensive atlas of the adult human brain transcriptome. *Nature* **489**, 391–399 (2012).
17. Miller, J. A. *et al.* Improving reliability and absolute quantification of human brain microarray data by filtering and scaling probes using RNA-Seq. *BMC Genomics* **15**, 154 (2014).
18. Fisher, R. A. *Statistical methods for research workers*. (Oliver and Boyd, 1925).
19. Benjamini, Y. & Hochberg, Y. Controlling the False Discovery Rate: A Practical and Powerful Approach to Multiple Testing. *J. R. Stat. Soc. Series B Stat. Methodol.* **57**, 289–300 (1995).
20. Ashburner, M. *et al.* Gene ontology: tool for the unification of biology. The Gene Ontology Consortium. *Nat. Genet.* **25**, 25–29 (2000).
21. Carlson, M. GO.db: A set of annotation maps describing the entire Gene Ontology. (2016).
22. Carlson, M. org.Hs.eg.db: Genome wide annotation for Human. (2016).
23. Supek, F., Bošnjak, M., Škunca, N. & Šmuc, T. REVIGO summarizes and visualizes long lists of gene ontology terms. *PLoS One* **6**, e21800 (2011).
24. Ogan, M. B. *et al.* Cross-Laboratory Analysis of Brain Cell Type Transcriptomes with Applications to Interpretation of Bulk Tissue Data. *eNeuro* ENEURO.0212–17.2017 (2017).
25. Darmanis, S. *et al.* A survey of human brain transcriptome diversity at the single cell level. *Proc. Natl. Acad. Sci. U. S. A.* **112**, 7285–7290 (2015).
26. Zeisel, A. *et al.* Molecular Architecture of the Mouse Nervous System. *Cell* **174**, 999–1014.e22 (2018).
27. O'Leary, N. A. *et al.* Reference sequence (RefSeq) database at NCBI: current status, taxonomic expansion, and functional annotation. *Nucleic Acids Res.* **44**, D733–45 (2016).

28. Keren-Shaul, H. *et al.* A Unique Microglia Type Associated with Restricting Development of Alzheimer's Disease. *Cell* vol. 169 1276–1290.e17 (2017).
29. Mathys, H. *et al.* Single-cell transcriptomic analysis of Alzheimer's disease. *Nature* **570**, 332–337 (2019).
30. Grothe, M. J. *et al.* Molecular properties underlying regional vulnerability to Alzheimer's disease pathology. *Brain* **141**, 2755–2771 (2018).
31. French, L. & Paus, T. A FreeSurfer view of the cortical transcriptome generated from the Allen Human Brain Atlas. *Front. Neurosci.* **9**, 323 (2015).
32. Hawrylycz, M. *et al.* Canonical genetic signatures of the adult human brain. *Nat. Neurosci.* **18**, 1832–1844 (2015).
33. Ritchie, J., Pantazatos, S. P. & French, L. Transcriptomic characterization of MRI contrast with focus on the T1-w/T2-w ratio in the cerebral cortex. *Neuroimage* (2018) doi:10.1016/j.neuroimage.2018.03.027.
34. Guillozet, A. L., Weintraub, S., Mash, D. C. & Mesulam, M. M. Neurofibrillary tangles, amyloid, and memory in aging and mild cognitive impairment. *Arch. Neurol.* **60**, 729–736 (2003).
35. Oddo, S. The ubiquitin-proteasome system in Alzheimer's disease. *J. Cell. Mol. Med.* **12**, 363–373 (2008).
36. Dominy, S. S. *et al.* Porphyromonas gingivalis in Alzheimer's disease brains: Evidence for disease causation and treatment with small-molecule inhibitors. *Sci Adv* **5**, eaau3333 (2019).
37. Singhrao, S. K. & Olsen, I. Assessing the role of Porphyromonas gingivalis in periodontitis to determine a causative relationship with Alzheimer's disease. *J. Oral Microbiol.* **11**, 1563405 (2019).

38. Lundmark, A. *et al.* Gene expression profiling of periodontitis-affected gingival tissue by spatial transcriptomics. *Sci. Rep.* **8**, 9370 (2018).

39. Ludden, C. W. Transcriptomic evaluation of peri-implant soft tissue in health and disease. (The Ohio State University, 2015).

40. Mesulam, M. M., Mufson, E. J., Wainer, B. H. & Levey, A. I. Central cholinergic pathways in the rat: an overview based on an alternative nomenclature (Ch1-Ch6). *Neuroscience* **10**, 1185–1201 (1983).

41. Sims, N. R. *et al.* Presynaptic cholinergic dysfunction in patients with dementia. *J. Neurochem.* **40**, 503–509 (1983).

42. Hampel, H. *et al.* Revisiting the Cholinergic Hypothesis in Alzheimer's Disease: Emerging Evidence from Translational and Clinical Research. *The Journal of Prevention of Alzheimer's Disease* **6**, 2–15 (2019).

43. DeKosky, S. T. *et al.* Cortical biopsy in Alzheimer's disease: diagnostic accuracy and neurochemical, neuropathological, and cognitive correlations. Intraventricular Bethanecol Study Group. *Ann. Neurol.* **32**, 625–632 (1992).

44. Sperling, R., Mormino, E. & Johnson, K. The evolution of preclinical Alzheimer's disease: implications for prevention trials. *Neuron* **84**, 608–622 (2014).

45. Lee, H. K., Hsu, A. K., Sajdak, J., Qin, J. & Pavlidis, P. Coexpression analysis of human genes across many microarray data sets. *Genome Res.* **14**, 1085–1094 (2004).

46. Gillis, J. & Pavlidis, P. The impact of multifunctional genes on 'guilt by association' analysis. *PLoS One* **6**, e17258 (2011).

47. Crow, M., Lim, N., Ballouz, S., Pavlidis, P. & Gillis, J. Predictability of human differential gene expression. *Proc. Natl. Acad. Sci. U. S. A.* **116**, 6491–6500 (2019).

48. Ding, Q., Markesbery, W. R., Chen, Q., Li, F. & Keller, J. N. Ribosome dysfunction is an

early event in Alzheimer's disease. *J. Neurosci.* **25**, 9171–9175 (2005).

49. Sajdel-Sulkowska, E. M. & Marotta, C. A. Alzheimer's disease brain: alterations in RNA levels and in a ribonuclease-inhibitor complex. *Science* **225**, 947–949 (1984).
50. Langstrom, N. S., Anderson, J. P., Lindroos, H. G., Winblad, B. & Wallace, W. C. Alzheimer's disease-associated reduction of polysomal mRNA translation. *Brain Res. Mol. Brain Res.* **5**, 259–269 (1989).
51. Hernández-Ortega, K., Garcia-Esparcia, P., Gil, L., Lucas, J. J. & Ferrer, I. Altered Machinery of Protein Synthesis in Alzheimer's: From the Nucleolus to the Ribosome. *Brain Pathol.* **26**, 593–605 (2016).
52. Koren, S. A. *et al.* Tau drives translational selectivity by interacting with ribosomal proteins. *Acta Neuropathol.* **137**, 571–583 (2019).
53. Meier, S. *et al.* Pathological Tau Promotes Neuronal Damage by Impairing Ribosomal Function and Decreasing Protein Synthesis. *J. Neurosci.* **36**, 1001–1007 (2016).
54. Moir, R. D., Lathe, R. & Tanzi, R. E. The antimicrobial protection hypothesis of Alzheimer's disease. *Alzheimers. Dement.* **14**, 1602–1614 (2018).
55. Dorn, B. R., Dunn, W. A., Jr & Progulske-Fox, A. Porphyromonas gingivalis traffics to autophagosomes in human coronary artery endothelial cells. *Infect. Immun.* **69**, 5698–5708 (2001).
56. Lee, K., Roberts, J. S., Choi, C. H., Atanasova, K. R. & Yilmaz, Ö. Porphyromonas gingivalis traffics into endoplasmic reticulum-rich-autophagosomes for successful survival in human gingival epithelial cells. *Virulence* **9**, 845–859 (2018).
57. Bélanger, M., Rodrigues, P. H., Dunn, W. A., Jr & Progulske-Fox, A. Autophagy: a highway for Porphyromonas gingivalis in endothelial cells. *Autophagy* **2**, 165–170 (2006).
58. Lempiäinen, H. & Shore, D. Growth control and ribosome biogenesis. *Curr. Opin. Cell Biol.*

21, 855–863 (2009).

59. Balderhaar, H. J. K. & Ungermann, C. CORVET and HOPS tethering complexes - coordinators of endosome and lysosome fusion. *J. Cell Sci.* **126**, 1307–1316 (2013).
60. How, K. Y., Song, K. P. & Chan, K. G. Porphyromonas gingivalis: An Overview of Periodontopathic Pathogen below the Gum Line. *Front. Microbiol.* **7**, 53 (2016).
61. Whitehouse, P. J. *et al.* Alzheimer's disease and senile dementia: loss of neurons in the basal forebrain. *Science* **215**, 1237–1239 (1982).
62. Whitehouse, P. J., Price, D. L., Clark, A. W., Coyle, J. T. & DeLong, M. R. Alzheimer disease: evidence for selective loss of cholinergic neurons in the nucleus basalis. *Ann. Neurol.* **10**, 122–126 (1981).
63. Mesulam, M., Shaw, P., Mash, D. & Weintraub, S. Cholinergic nucleus basalis tauopathy emerges early in the aging-MCI-AD continuum. *Ann. Neurol.* **55**, 815–828 (2004).
64. Kato, T. *et al.* The effect of the loss of molar teeth on spatial memory and acetylcholine release from the parietal cortex in aged rats. *Behav. Brain Res.* **83**, 239–242 (1997).
65. Onozuka, M., Watanabe, K., Fujita, M., Tomida, M. & Ozono, S. Changes in the septohippocampal cholinergic system following removal of molar teeth in the aged SAMP8 mouse. *Behav. Brain Res.* **133**, 197–204 (2002).
66. Avivi-Arber, L. *et al.* Widespread Volumetric Brain Changes following Tooth Loss in Female Mice. *Front. Neuroanat.* **10**, 121 (2016).
67. Grothe, M. J., Heinsen, H., Amaro, E., Jr, Grinberg, L. T. & Teipel, S. J. Cognitive Correlates of Basal Forebrain Atrophy and Associated Cortical Hypometabolism in Mild Cognitive Impairment. *Cereb. Cortex* **26**, 2411–2426 (2016).
68. Dobbertin, A. *et al.* Targeting of acetylcholinesterase in neurons in vivo: a dual processing function for the proline-rich membrane anchor subunit and the attachment domain on the

catalytic subunit. *J. Neurosci.* **29**, 4519–4530 (2009).

69. Han, X. *et al.* Loss of nitrergic and cholinergic neurons in the enteric nervous system of APP/PS1 transgenic mouse model. *Neurosci. Lett.* **642**, 59–65 (2017).
70. Kaur, G. & Levy, E. Cystatin C in Alzheimer's disease. *Front. Mol. Neurosci.* **5**, 79 (2012).
71. Olsen, I. & Potempa, J. Strategies for the inhibition of gingipains for the potential treatment of periodontitis and associated systemic diseases. *J. Oral Microbiol.* **6**, (2014).
72. Sharma, A., Pradeep, A. R., Raghavendra, N. M., Arjun, P. & Kathariya, R. Gingival crevicular fluid and serum cystatin c levels in periodontal health and disease. *Dis. Markers* **32**, 101–107 (2012).
73. Abrahamson, M., Wikström, M., Potempa, J., Renvert, S. & Hall, A. Modification of cystatin C activity by bacterial proteinases and neutrophil elastase in periodontitis. *Mol. Pathol.* **50**, 291–297 (1997).
74. Blankenvoorde, M. F. *et al.* Cystatin and cystatin-derived peptides have antibacterial activity against the pathogen Porphyromonas gingivalis. *Biol. Chem.* **379**, 1371–1375 (1998).
75. Jansen, I. E. *et al.* Genome-wide meta-analysis identifies new loci and functional pathways influencing Alzheimer's disease risk. *Nat. Genet.* **51**, 404–413 (2019).
76. N'Diaye, E.-N. *et al.* TREM-2 (triggering receptor expressed on myeloid cells 2) is a phagocytic receptor for bacteria. *J. Cell Biol.* **184**, 215–223 (2009).